

Reordering of Depolymerized Silicates as Adsorbents for Large Nitrogen Compounds

Norma A. Sánchez-Flores,^{✉*}^a Juan Navarrete-Bolaños,^b Patricia Pérez-Romo,^b
Graciela Pacheco-Malagón,^a Georgina Laredo[✉]^b and José J. Fripiat^{†,a}

^aInstituto de Ciencias Aplicadas y Tecnología, Universidad Nacional Autónoma de México,
Circuito Exterior s/n, Ciudad Universitaria, CP 04510, Mexico City, Mexico

^bInstituto Mexicano del Petróleo, Eje Central Lázaro Cárdenas No. 152,
Col. San Bartolo Atepehuacan, CP 07730, Mexico City, Mexico

The adsorption capacities of two synthesized zeolites (crystalline ZSM-5 and semi-crystalline faujasite Y) for a mixture of indole, quinoline and carbazole were studied. The different samples obtained show different crystalline degree, mesoporosity and Si/Al ratios. The synthesis procedure is based on the simultaneous depolymerization of a mixture of high surface area silica, such as rice hull ashes (RHA), and a crystalline zeolite, such as clinoptilolite or faujasite. The depolymerization step is followed by a partial reorganization induced by a structure-directing agent. A model mixture of nitrogenous compounds was prepared, then it was mixed with the zeolite samples and the amount adsorbed of nitrogenous compounds was determined by gas chromatography. Analysis of the adsorbed molecules reveals selectivity in favor of quinoline, followed by indole and then carbazole. The best adsorbent properties correspond to the solid with highest porous volume. The samples obtained were characterized by X-ray diffraction, ²⁹Si and ²⁷Al magic-angle spinning nuclear magnetic resonance, X-ray fluorescence and Fourier transform infrared spectroscopy. The Barrett-Joyner-Halenda (BJH) pore size distribution and the Brunauer-Emmet-Teller (BET) surface area values were obtained from N₂ adsorption/desorption isotherms.

Keywords: nitrogen compound adsorption, rice hull ash, ZSM-5, faujasite Y

Introduction

The production of ultralow sulfur diesel (ULSD) is imperative worldwide due to current air pollution. Several environmental regulations have been established to achieve ultradeep hydrodesulfurization (HDS).¹

Some basic nitrogen compounds exert an inhibiting effect when absorbed into the acid sites of HDS catalysts, while neutral compounds are prone to form gums that block the catalyst pores.²⁻⁴ In this sense, nitrogenous compounds present in straight run gas oil (SRGO), coker gas oil (CGO) and light cycle oil (LCO), which are used as feedstocks for diesel fuel production, have been identified as strong inhibitors of HDS reactions due to catalyst poisoning. Therefore, elimination of these compounds is crucial to reaching the low sulfur levels that are required for fuels.

The nitrogenous compounds found in gas oil are generally divided into two groups: basic compounds, such

as aniline, pyridine, quinoline, acridine and their alkyl derivatives, and nonbasic compounds, such as pyrrole, indole, carbazole, and their alkyl derivatives. Due to the diversity of nitrogenous compounds, great interest has been focused on the study of different adsorbents for the selective removal of these compounds.⁵⁻¹⁴ The pretreatment of gas oil to remove nitrogenous compounds using silica, silica-alumina, activated carbon and zeolites has been proposed.¹⁴⁻¹⁶

Rice hull is an agricultural waste that is widely used to produce amorphous silica by physical combustion at controlled temperatures and has been used for synthesizing advanced materials such as SiO₂, SiC, Si₃N₄, elemental Si, Mg₂Si and active carbon.¹⁷ On the other hand, different zeolites have been synthesized using the silica from rice hull, usually under hydrothermal conditions from solutions of sodium silicate.^{18,19}

In this sense, extensive work has been carried out on the syntheses of ZSM-5²⁰⁻²⁴ and Y zeolite²⁵⁻³⁰ with rice hull ash (RHA) as the source of silica. When rice hull is used as a silica and aluminum source, a highly siliceous ZSM-5

*e-mail: norma.sanchez@icat.unam.mx

[†]In memoriam.

(silicalite) is obtained.³¹⁻³³ Additionally, a template-free synthesis of ZSM-5 has been reported.³⁴⁻³⁶ With an external aluminum source, such as aluminum sulfate³⁷ or sodium aluminate,³⁸⁻⁴⁰ ZSM-5 samples with a micro-mesoporous nature have been obtained. However, a mesoporous Y zeolite has not been reported.

A novel technique for the preparation of mesoporous adsorbents using gels obtained from depolymerized silicates has been reported by our group.⁴¹⁻⁴⁶ This technique first involves the simultaneous depolymerization of a mixture of high-surface-area silica, such as rice hull ash (RHA), and of a crystalline zeolite, such as clinoptilolite or faujasite. This step is followed by partial reorganization induced by a structure-directing agent (SDA). While the simultaneous depolymerization of two silica sources, RHA and zeolite, silicate is enriched in silica, and the supplementary silica is not distributed at random; it is most likely attached to the dangling bonds of the attacked zeolite network and forms a porous material that is supported by the structured residue of the silica. Pacheco-Malagón *et al.*⁴³ have worked with ZSM-5 synthesized from residual rice hull.

In this contribution, emphasis is placed on the adsorption of large nitrogenous molecules that behave as poisons to HDS catalysts. The concept involves grafting porous siliceous materials onto a thermally stable network (zeolite) for the affordable synthesis of adsorbents capable of removing unwanted nitrogenous molecules.

Experimental

Materials

Three raw materials were used: rice hull ashes, natural clinoptilolite and acid faujasite CBV 720 by Zeolyst International (Kansas City, USA). Rice hull from Morelos, Mexico, were heated in air at 500 °C for 24 h to obtain RHA.⁴⁵ Clinoptilolite from San Luis Potosi, Mexico, was milled, exchanged with a 0.1 M NH₄Cl solution several times at room temperature and washed and purified several times by decantation.⁴⁴ Tetrapropylammonium hydroxide (TPA) and tetramethylammonium hydroxide (TMA) were acquired from Sigma-Aldrich (Toluca, Mexico).

Synthesis

Two series of samples were prepared: (i) from a mixture clinoptilolite and RHA that yielded the crystalline zeolite type ZSM-5 (ZSM samples) and (ii) using seeds of a well-crystallized faujasite Y and RHA that produced the semi-crystalline zeolite type faujasite Y (YRHA samples) (Table 1). The two-step preparation consisted of treating

the starting solid mixture with 10 mL of anhydrous glycerol *per g* at 200 °C, 2 h for the ZSM samples and 3 h for the YRHA samples under continuous stirring. An amorphous organo-silicic gel was formed and was cooled to 50 °C. The gel was hydrolyzed with TPA to obtain ZSM-5 (1.7 mL of a 1 M TPA solution *per g* and 5.1 mL of distilled water) or TMA for faujasite (0.06 g of TMA *per g* and 3.3 mL of distilled water). The gel was further aged in a cylindrical stainless steel reactor (100 mL capacity) to initiate a partial structural reorganization of the solid under autogenous pressure at 135 °C for 72 h for ZSM samples and 95 °C for 12 h for YRHA samples. Finally, the solid residue was washed by centrifugation three times at 5000 rpm, dried at 100 °C for 24 h, and calcined at 500 °C for 24 h.

Table 1. Clinoptilolite and faujasite content in the preparation of samples labeled ZSM (ZSM-5) and YRHA (faujasite Y) with rice hull ash (RHA)

Sample	Clinoptilolite / wt. %	RHA / wt. %
ZSM-1	14	86
ZSM-2	20	80
ZSM-3	25	75
ZSM-4	33	67
Faujasite / wt. %		
YRHA-1	12.5	87.5
YRHA-2	25	75
YRHA-3	37.5	62.5

Adsorption

Batch adsorption experiments were conducted for the powdered ZSM and YRHA samples in a beaker flask with a water-bath jacket. The temperature, pressure and stirring rate were set to 35 °C, 0.078 MPa and 330 rpm, respectively.

A model mixture was prepared by dissolving 53, 27 and 27 mg of quinolone, indole and carbazole, respectively, in 10 mL (8.03 g) of a toluene/hexadecane mixture (1/1 v/v) to achieve final concentrations of each nitrogen compound of 41, 23 and 16 mmol L⁻¹. Next, 10 mL of this mixture was mixed with 1 g of sample and stirred at room temperature. Equilibrium data were obtained after 2 h of contact time, the solid was separated from the liquid by filtration. The content of nitrogenous compounds was determined by gas chromatography on a Bruker 450-GC model equipped with a pulsed photometric detector (PFPD) under He flow at 350 °C and a 50 m × 0.32 mm × 0.32 μm fused silica capillary column coated with Bruker phase BR-5 (BR29730)d. The adsorption capacity was calculated from the difference between the initial and equilibrium

concentrations of nitrogen compounds and corresponded to the analyzed pure nitrogen compounds.

Characterization

The ^{29}Si magic-angle spinning nuclear magnetic resonance (MAS NMR) spectra were obtained at 79.492 MHz on a Bruker Advance 400; spinning zirconia rotors (4 mm internal diameter, at 7.5 kHz, 90° pulses in 20 s intervals) were used. The number of transients was 250. ^{27}Al MAS NMR spectra were also recorded. The NMR spectrum deconvolution was achieved using Origin 7 software.⁴⁷

The X-ray diffraction (XRD) analyses of the samples were recorded with Siemens D-5000 equipment, which was fitted with a graphite secondary beam monochromator to filter Cu K α radiation. X-ray diffractograms were recorded from 4 to 70° with 2θ steps of 0.02° and a 1.8 s counting time.

The chemical composition was determined by X-ray fluorescence (XRF) with XRF Siemens SRS300 fluorometer with a Rh tube and a 125 μm Be window. The samples preparation technique was the fusion method, using metaborate and lithium tetraborate.

The textural properties of the evaluated solids were determined by nitrogen adsorption-desorption isotherms at 77 K with a Quantachrome Automated Gas Sorption System. The samples were previously outgassed under vacuum (1.33×10^{-10} MPa) at 573 K (CDX and SG) and 473 K (VG-077) for 18 h. The pore size distribution was calculated from the adsorption branch according to the Barrett-Joyner-Halenda (BJH) method, and the Brunauer-Emmet-Teller (BET) model was used for calculating the total surface area of the solids.

Indole adsorption was monitored by Fourier transform infrared spectroscopy (FTIR) using a Nicolet 710

spectrometer. The spectra were obtained from self-supported sample pressed discs placed in a Pyrex cell equipped with CaF_2 windows. Before the tests, the samples were outgassed at 673 K under vacuum. The active solid content in the discs was sufficient to provide IR spectra of good quality.

For FTIR study of nitrogen compound interactions, the indole was adsorbed at room temperature and progressively desorbed at different temperatures under vacuum. The temperature programming was as follows. First, the sample was heated at 400 $^\circ\text{C}$ in the vacuum system (activated sample). Afterwards, the temperature was lowered to room temperature, indole was introduced to the sample (pressed disc), and a second spectrum was recorded (Indole TA). To remove the indole, the temperature was increased to 300 $^\circ\text{C}$ while spectra were recorded at different temperatures.

Results and Discussion

Zeolite samples type MFI (ZSM-5)

The following results were obtained by increasing the amount of clinoptilolite mixed with RHA in the starting material mixture and hydrolyzing with TPA. The main textural characteristics determined from the low temperature N_2 adsorption-desorption isotherms are the pore volume (cc g^{-1}) and surface area ($\text{m}^2 \text{g}^{-1}$). For clinoptilolite, with relative contents between 14 (ZSM-1) and 33% (ZSM-4), the surface areas fluctuate from 330 to $227 \text{ m}^2 \text{g}^{-1}$ and the porous volume varies from 0.14 to 0.13 cc g^{-1} , respectively (Table 2). The results of the chemical analysis show that the aluminum content increases according to the increase in the clinoptilolite content in the synthesis (Table 3). Impurities such as K_2O , CaO and Fe_2O_3 originate from the clinoptilolite and RHA.

Table 2. Properties of the samples derived from rice hull ash and clinoptilolite

Sample	nSi/nAl	BET ^a surface area / ($\text{m}^2 \text{g}^{-1}$)	Total pore volume / (cc g^{-1})	Average pore size / Å	XRD ^b crystallinity / %
ZSM-1	39.69	330.3	0.1404	16.89	73.5
ZSM-2	30.21	315.7	0.1312	16.84	71.7
ZSM-3	25.42	299.6	0.127	16.89	68.5
ZSM-4	19.69	227.2	0.133	17.54	67.5

^aBET surface area: according to Brunauer-Emmet-Teller theory; ^bXRD crystallinity: calculated from X-ray diffraction pattern.

Table 3. Chemical analysis of the ZSM samples

Sample	SiO_2 / wt.%	Al_2O_3 / wt.%	Na_2O / wt.%	CaO / wt.%	K_2O / wt.%	MgO / wt.%	Fe_2O_3 / wt.%
ZSM-1	95.08	2.03	0.05	0.48	1.34	0.40	0.34
ZSM-2	93.50	2.63	0.10	0.78	1.78	0.41	0.42
ZSM-3	92.45	3.09	0.05	0.90	2.11	0.46	0.49
ZSM-4	90.64	3.91	0.16	1.03	2.80	0.45	0.63

Solids may be assumed to contain a homogeneous distribution of micropores (zeolitic pores) within a system of mesopores of identical chemical composition (Figure 1). One could imagine fragmented zeolite networks encased by a porous system of larger cavities. The choice of ZSM-5 was based on the toughness of its lattice and on previously published work.⁴³

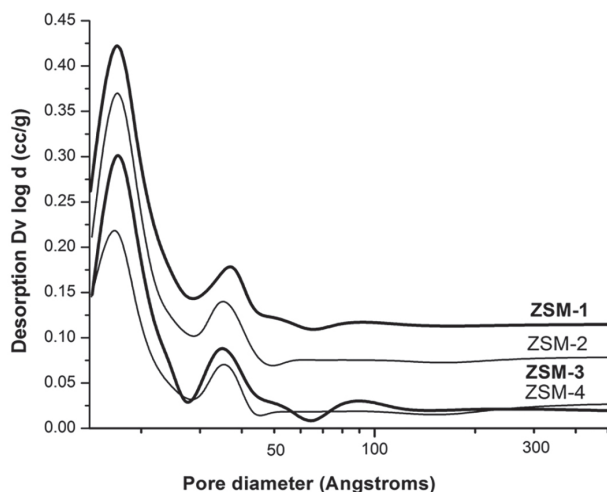


Figure 1. Mesopore diameter distribution of zeolite type ZSM-5.

The silicon and aluminum NMR spectra (Figures 2 and 3) reveal some fundamental characteristics of the process used to prepare these adsorbents. The ²⁹Si NMR spectra show three peaks upon deconvolution; the first and second peaks were assigned to Q⁴ cluster resonances (−113 and −115 ppm), and the third at −104 ppm corresponds to Q³ clusters. The Q⁴ resonance signal shows the fourfold coordination of silicon to oxygen with a varying Si–O–Si angle (Table 4).⁴⁸ The small peak that emerged in the Q³ region increased with increasing clinoptilolite content, probably because of the contribution of aluminum. On the other hand, ²⁷Al NMR spectra show the presence of only one peak at 55.5 ppm, attributed to a tetrahedral structure, while no octahedral aluminum was detected (Figure 3).

After depolymerization, hydrolysis and aging, only a four-fold coordinated aluminum combined with silicon is observable, and the XRD pattern does not show diffraction

Table 4. ²⁹Si chemical shifts of the Q⁴ and Q³ clusters for the ZSM samples

Sample	Q ⁴	Intensity ^a / %	Q ⁴	Intensity ^a / %	Q ³	Intensity ^a / %
ZSM-1	−115.6	31.0	−113.3	64.3	−104.3	4.7
ZSM-2	−115.9	33.3	−113.2	59.8	−104.1	6.9
ZSM-3	−115.3	35.8	−113.1	53.3	−104.5	10.9
ZSM-4	−115.5	37.5	−113.2	50.1	−104.9	12.4

^aRelative intensity.

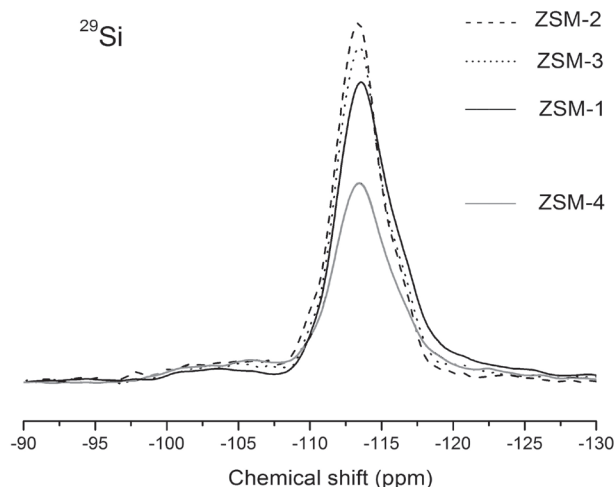


Figure 2. ²⁹Si NMR spectra of the ZSM samples.

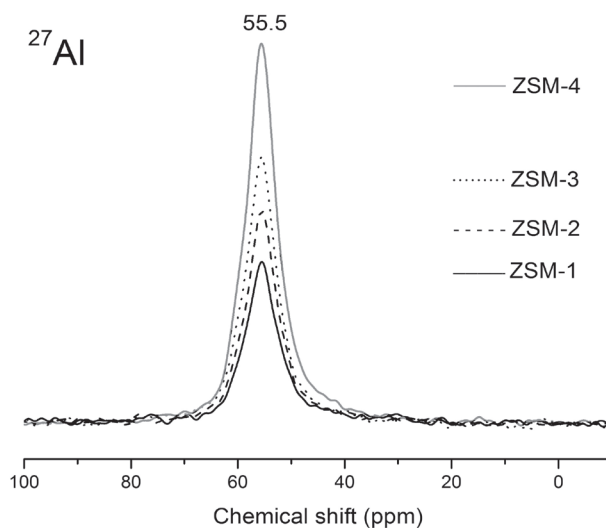


Figure 3. ²⁷Al NMR spectra of the ZSM samples.

lines other than those attributable to the MFI framework (Figure 4).

Zeolite samples type faujasite

The faujasite lattice is not as condensed as that of MFI. Three samples coded YRHA-1, YRHA-2 and YRHA-3 were prepared, their chemical analysis is reported on Table 5. Here the structural backbone is a faujasite

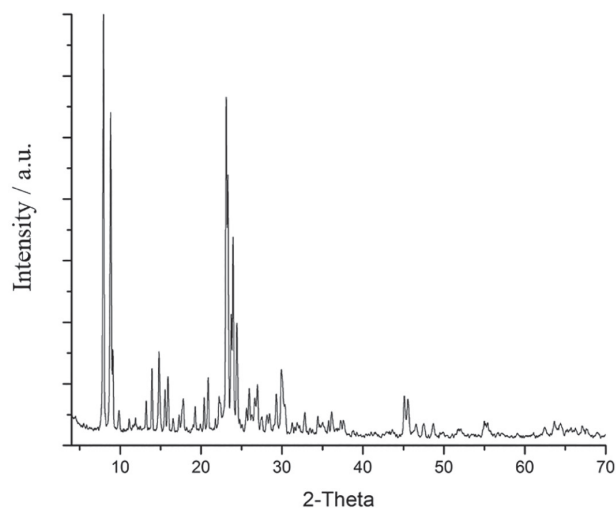


Figure 4. Diffraction pattern of the ZSM-1 sample.

synthesized from a relative amount of NaY between 12.5 and 37.5% (Table 1). The XRD pattern shows diffraction lines assigned to faujasite and halos due to amorphous silicon (Figure 5). Mesoporosity is characteristic in these samples (Figure 6).

Approximately 27% of the Y-type zeolite could be crystallized by this method, with a surface area between 169 and 258 m² g⁻¹ and a large pore size ranging from 73 to 95 Å without an apparent correlation with the Si/Al ratio. These results show that the residual silica greatly increased its textural properties, enabling the preparation of materials with large pore (samples YRHA-2 and YRHA-3) (Table 6).

Interactions between selected molecules and the adsorbents

It is necessary to determine whether selective adsorption occurs with respect to molecular shape or with respect to the adsorbent. For this purpose, a mixture of molecules was used for the ZSM and YRHA adsorption studies. A mixture

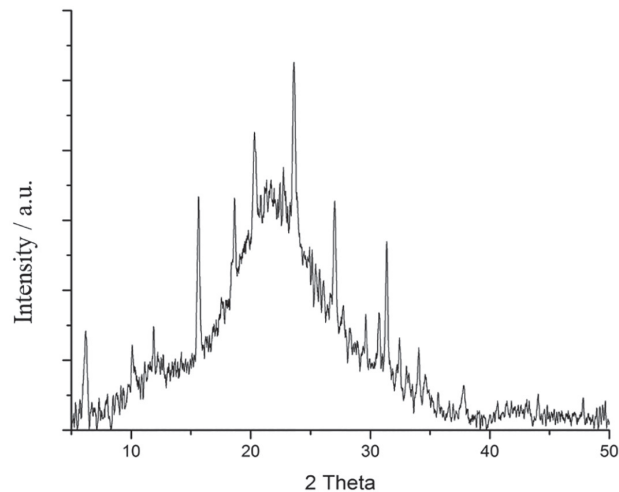


Figure 5. Diffraction pattern of the YRHA-2 sample.

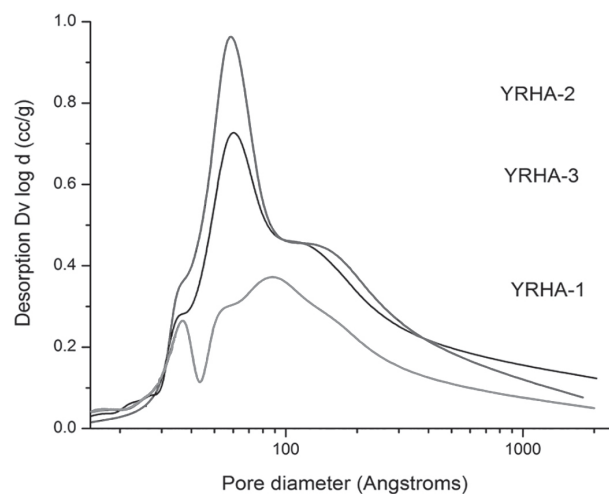


Figure 6. Mesopore diameter distribution of the YRHA samples.

of basic (quinoline) and neutral (indole and carbazole) nitrogen molecules was used. The chosen model molecules were heterocycles with 2 or 3 rings, the carbazole molecule is the largest (Table 7).

Table 5. Chemical analysis of the YRHA samples

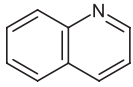
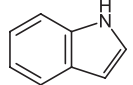
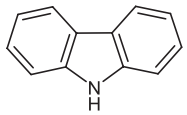
Sample	SiO ₂ / %	Al ₂ O ₃ / %	Na ₂ O / %	CaO / %	K ₂ O / %	MgO / %	Fe ₂ O ₃ t / %
YRHA-1	92.95	3.16	0.72	0.38	1.03	0.34	0.12
YRHA-2	87.22	7.88	2.80	0.40	1.00	0.35	0.12
YRHA-3	90.68	5.62	1.55	0.42	1.00	0.40	0.12

Table 6. Properties of the samples derived from rice hull ash and faujasite

Sample	nSi/nAl	BET ^a surface area / (m ² g ⁻¹)	Total pore volume / (cc g ⁻¹)	Average pore size / Å	XRD ^b crystallinity / %
YRHA-1	24.99	169.5	0.31	73.2	25
YRHA-2	9.75	255.7	0.59	83.5	29
YRHA-3	13.71	257.7	0.61	94.9	24

^aBET surface area: according to Brunauer-Emmet-Teller theory; ^bXRD crystallinity: calculated from X-ray diffraction pattern.

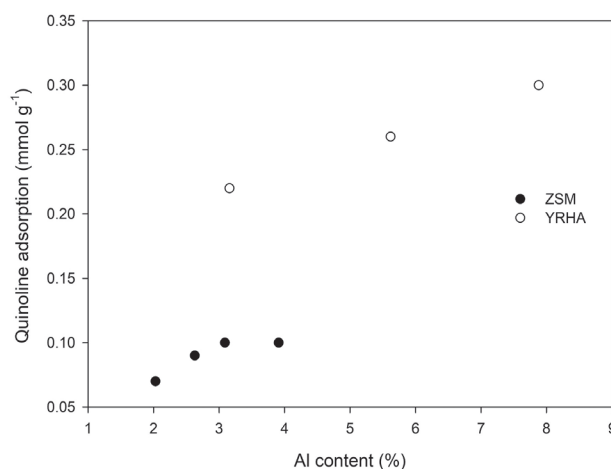
Table 7. Characteristic properties of model molecules used

Molecule	Configuration	p <i>K_a</i>	Surface covered / Å ²	Melting point / °C
Quinoline		4.85	156.61	-15
Indole		16.2	150.76	52.54
Carbazole		19.2	195.8	246.3

Analysis of the adsorbed molecules (Table 8) compared to the initial composition reveals some significant selectivity in favor of quinoline, followed by indole and then carbazole, indicating the relative acidic character of the solids despite not being in their acid form. Basic nitrogen compounds compete for the acid sites, while the adsorption of neutral nitrogen compounds occurs through H-bonding and π -electron interactions.⁴⁹ Figure 7 shows the increase in quinoline adsorption in response to an increase in aluminum content, which is responsible for the acidity in the samples.

The adsorption of the nitrogenous model molecule compounds by the YRHA samples is greater than those reported for the ZSM samples. ZSM-3 and YRHA-1 with similar composition show that the adsorption capacity is most probably because of the larger pore volumes and pore sizes in the former. Among the adsorbents examined, the best appears to be YRHA-2, which is the one with the highest porous volume (Table 6).

Contact with the adsorbent removed between 0.15 and 0.44 mmol g⁻¹ from 0.80 mmol g⁻¹ added. It is evident that the density of the starting material plays an important role and should be investigated more thoroughly.

**Figure 7.** Quinoline adsorption on the ZSM and YRHA samples as a function of the Al content.

Infrared study

The trend revealed by the comparison of the two categories of adsorbents is encouraging. The surface chemical compositions of these adsorbents should only differ by the concentration of the chemical components. This aspect deserves more attention and will be studied using a molecular probe and infrared spectroscopy. Indole

Table 8. Adsorption capacity comparison between the adsorbents obtained

Sample	Quinoline / (mmol g ⁻¹)	Indole / (mmol g ⁻¹)	Carbazole / (mmol g ⁻¹)	Total (± 0.003) / (mmol g ⁻¹)
Initial content	0.41	0.23	0.16	0.80
ZSM-1	0.07	0.04	0.04	0.15
ZSM-2	0.09	0.04	0.05	0.18
ZSM-3	0.10	0.05	0.02	0.17
ZSM-4	0.10	0.05	0.05	0.20
YRHA-1	0.22	0.04	0.03	0.28
YRHA-2	0.30	0.08	0.06	0.44
YRHA-3	0.26	0.07	0.05	0.38

is an excellent IR probe because of the N–H bond in the pentagonal ring. Moreover, indole is one of the molecules that poisons the catalysts.

The N–H vibration bands of indole are extremely sensitive to interactions with O–H or chemisorbed water, as has been shown by Carney *et al.*⁵⁰ They described the hydrogen-bonding topologies of indole-(water)ⁿ clusters, where the N–H stretch at 3524 cm⁻¹ served as a reference for the indole-water cluster transitions. Thus, in spite of its complexity, it is possible to use the infrared spectrum of indole as a very rich source of information on its interactions with adsorbents.

The reactions of indole with these surfaces are different from what was expected. On silica gel, the reactivity mainly involves surface silanols. The intensity of the O–H stretching decreases as the amount of desorbed

indole increases. This observation implies a decrease in the number of hydrogen-bonded O–H as well as a slight high frequency shift. On the sample, the dominant indole bands near 3600 and 3420 cm⁻¹ exhibit different behaviors.

Fourier transform infrared spectroscopy (FTIR) of surfaces is a common tool utilized to study interactions between solids and molecules linked through the hydroxyl groups (i.e., indole). Considering the samples with higher adsorption capacities, Figures 8 and 9 display the FTIR spectra of the adsorbed species arising from the contact of YRHA-2 and ZSM-4 with indole. For ZSM-4, a saturation signal is observed in the region from 3800 to 3200 cm⁻¹, indicating an excess of indole was adsorbed. In both series of spectra, the indole adsorption formed strong broad adsorption bands in the region from 3650 to 3250 cm⁻¹. This band formed at the expense of the signal attributed to

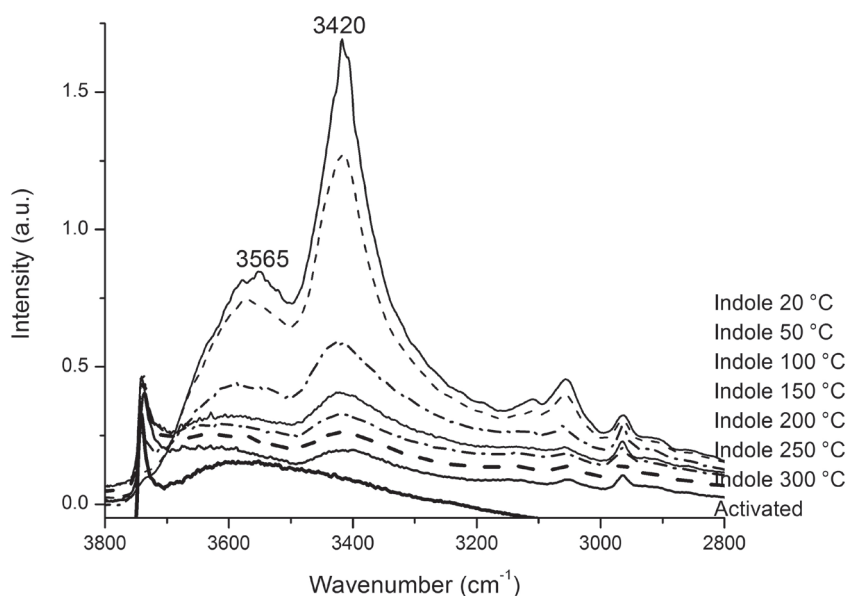


Figure 8. Infrared spectra of the adsorption-desorption behavior of indole on YRHA-2 at different temperatures.

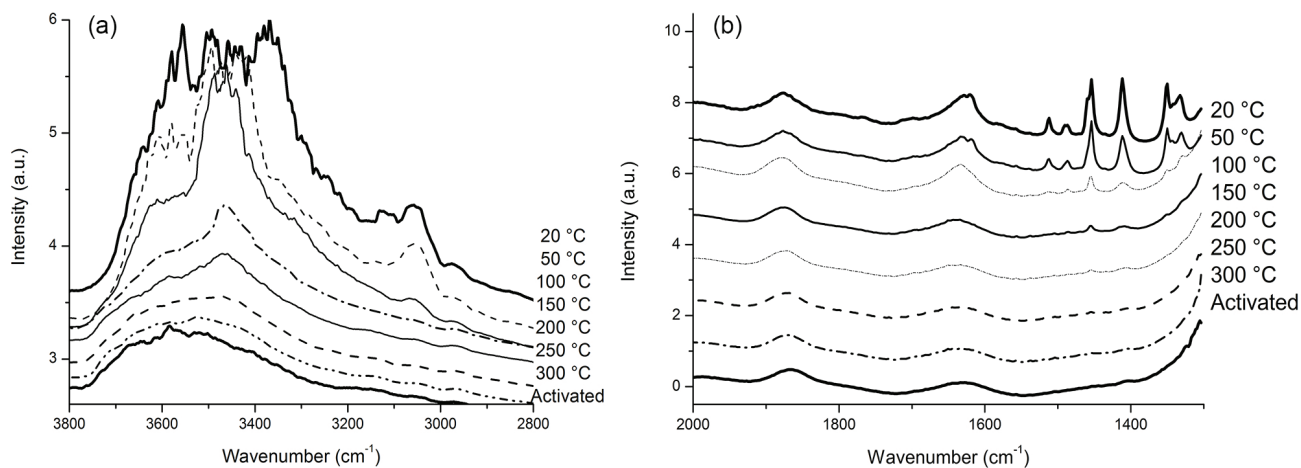


Figure 9. Infrared spectra of the adsorption-desorption of indole on ZSM-4 at different temperatures. The presence of indole is apparent in the ranges from 3800 to 3000 cm⁻¹ (a) and 1600 to 1300 cm⁻¹ (b).

surface hydroxyls, which is typically observed in the region from 3800 to 3200 cm^{-1} . This finding suggests that indole interacted with and perturbed the surface hydroxyl groups of YRHA-2 and ZSM-4 through hydrogen bonding. Though indole desorbed from ZSM-4 at 200 °C, its presence on YRHA-2 remained even at 300 °C; this finding suggests a stronger interaction with YRHA-2 and the formation of a surface complex. For ZSM-4, evidence of this complex is more clearly observed in the region from 1600 to 1300 cm^{-1} , where a weakening of the indole signal is evident.

That strong interaction on YRHA-2 was expected due to the acidic character of the surface hydroxyl. To assist in explaining the observed behavior of ZSM-4, which contained a lower aluminum content than YRHA-2, it is necessary to note the importance of acidity in the adsorption capacity of solids with a donor-acceptor component in the interaction (i.e., hydrogen bonding). The strongest adsorption of organic compounds occurred when the dehydrated surface presented isolated hydroxyl groups.

These results demonstrate that indole interacts with both YRHA-2 and ZSM-4 through hydrogen bonding. Additionally, both materials exhibit a higher affinity for quinoline than for indole.

On YRHA-2 and ZSM-4, the affinity for carbazole is slightly higher than that for indole despite the steric effect and the pore volume of the materials.

Conclusions

Contact with mesoporous semi-crystalline adsorbents removed around 55% of the components in a model mixture. Although the adsorption of large nitrogenous molecules was satisfactory for a proof-of-concept, there remains room for improvement. More than 90% of N-compounds should be eliminated by the adsorbent; however, the observed trends among the different solids are encouraging. It is evident that the density of the starting material plays important roles. The novel technique suggested here is promising and warrants further investigation.

Acknowledgments

In memory of a great researcher and teacher, but above all a great man and a great friend, José J. Fripiat.

We thank CONACYT for financial support (project 144141), Néstor R. Ortega from Instituto de Ciencias Aplicadas y Tecnología for contributing the experimental synthesis, Patricia Giron, from Instituto de Geología for contributing the X-ray fluorescence analysis and Adriana Tejada, from Instituto de Investigaciones en Materiales for

contributing the X-ray diffraction analysis, of Universidad Nacional Autónoma de México.

Author Contributions

José J. Fripiat was responsible for investigation (lead), formal analysis (lead) and writing original draft (lead); Norma A. Sánchez-Flores for investigation (lead), formal analysis (lead) and writing-review and editing (lead); Juan Navarrete-Bolaños for data curation (lead) and formal analysis (lead); Patricia Pérez-Romo for investigation (lead), formal analysis (lead) and writing-review and editing (supporting); Graciela Pacheco-Malagón for investigation (supporting), formal analysis (lead), data curation (lead); Georgina Laredo for investigation (lead), formal analysis (lead), and writing-review and editing (supporting).

References

1. Srivastava, V. C.; *RSC Adv.* **2012**, *2*, 759.
2. Jeong, D. S.; Massoth, F. E.; *Catal. Today* **1997**, *37*, 267.
3. Ramachandran, R.; Massoth, F. E.; *Chem. Eng. Commun.* **1982**, *18*, 239.
4. Muegge, B.; Massoth, F. E.; *Catalyst Deactivation*; Bartholomew, C. H.; Butt, J. B., eds.; Elsevier: Amsterdam, 1991.
5. Kim, J. H.; Ma, X.; Zhou, A.; Song, C.; *Catal. Today* **2006**, *111*, 74.
6. Min, W.; *Korean J. Chem. Eng.* **2002**, *19*, 601.
7. Thomas, J. K.; Gunda, K.; Rehbein, P.; Ng, F. T. T.; *Appl. Catal., B* **2010**, *94*, 225.
8. Laredo, G. C.; Vega-Merino, P. M.; Trejo-Zárraga, F.; Castillo, J.; *Fuel Process. Technol.* **2013**, *106*, 21.
9. Almarri, M.; Ma, X.; Song, C.; *Ind. Eng. Chem. Res.* **2009**, *48*, 951.
10. Rashidi, S.; Nikou, M. R. K.; Anvaripour, B.; *Microporous Mesoporous Mater.* **2015**, *211*, 134.
11. Mohammadian, M.; Ahmadi, M.; Khosravi-Nikou, M. R.; *Pet. Sci. Technol.* **2017**, *35*, 608.
12. Mohammadian, M.; Khosravi-Nikou, M. R.; Shariati, A.; Aghajani, M.; *Clean Technol. Environ. Policy* **2018**, *20*, 95.
13. Ahmadi, M.; Anvaripour, B.; Khosravi-Nikou, M. R.; Mohammadian, M.; *J. Environ. Chem. Eng.* **2017**, *5*, 849.
14. Hernandez-Maldonado, A. J.; Yang, R. T.; *Angew. Chem.* **2004**, *43*, 1004.
15. Infantes-Molina, A.; Moreno-León, C.; Pawelec, B.; Fierro, J. L. G.; Rodríguez-Castellón, E.; Jiménez-López, A.; *Appl. Catal., B* **2012**, *113-114*, 87.
16. Sano, Y.; Choi, K. H.; Korai, Y.; Mochida, I.; *Energy Fuels* **2004**, *18*, 644.
17. Soltani, N.; Bahrami, A.; Pech-Canul, M. I.; González, L. A.; *Chem. Eng. J.* **2015**, *264*, 899.

18. Hamdan, H.; Muhid, M. N. M.; Endud, S.; Listiorini, E.; Ramli, Z.; *J. Non-Cryst. Solids* **1997**, *211*, 126.
19. Sun, L.; Gong, K.; *Ind. Eng. Chem. Res.* **2001**, *40*, 5861.
20. Rawtani, A. V.; Rao, M. S.; Gokhale, K. V. G. K.; *Ind. Eng. Chem. Res.* **1989**, *28*, 1411.
21. Chareonpanich, M.; Namto, T.; Kongkachuichay, P.; Limtrakul, J.; *Fuel Process. Technol.* **2004**, *85*, 1623.
22. Ali, I. O.; Hassan, A. M.; Shaaban, S. M.; Soliman, K. S.; *Sep. Purif. Technol.* **2011**, *83*, 38.
23. Prasetyoko, D.; Ayunanda, N.; Fansuri, H.; Hartanto, D.; Ramli, Z.; *ITB J. Sci.* **2012**, *44A*, 250.
24. Kordatos, K.; Ntziouni, A.; Iliadis, L.; Kasselouri-Rigopoulou, V.; *J. Mater. Cycles Waste Manage.* **2013**, *15*, 571.
25. Wittayakun, J.; Khemthong, P.; Prayoonpokarach, S.; *Korean J. Chem. Eng.* **2008**, *25*, 861.
26. Yusof, A. M.; Nizam, N. A.; Rashid, N. A. A.; *J. Porous Mater.* **2010**, *17*, 39.
27. Tan, W. C.; Yap, S. Y.; Matsumoto, A.; Othman, R.; Yeoh, F. Y.; *Adsorption* **2011**, *17*, 863.
28. Saceda, J.-J. F.; de Leon, R. L.; Rintramee, K.; Prayoonpokarach, S.; Wittayakun, J.; *Quim. Nova* **2011**, *34*, 1394.
29. Rahman, M. M.; Awang, M. B.; Yusof, A. M.; *Adv. Mater. Res.* **2012**, *445*, 821.
30. Mohamed, R. M.; Mkhallid, I. A.; Barakat, M. A.; *Arabian J. Chem.* **2015**, *8*, 48.
31. Wang, H. P.; Lin, K. S.; Huang, Y. J.; Li, M. C.; Tsaur, L. K.; *J. Hazard. Mater.* **1998**, *58*, 147.
32. Kordatos, K.; Gavela, S.; Ntziouni, A.; Pistiolas, K. N.; Kyritsi, A.; Kasselouri-Rigopoulou, V.; *Microporous Mesoporous Mater.* **2008**, *115*, 189.
33. Katsuki, H.; Furuta, S.; Watari, T.; Komarneni, S.; *Microporous Mesoporous Mater.* **2005**, *86*, 145.
34. Fernandes, A. A.; Frajndlich, E. U.; Riella, H. G.; *Mater. Sci. Forum* **2005**, *499*, 676.
35. Vempati, R. K.; Borade, R.; Hegde, R. S.; Komarneni, S.; *Microporous Mesoporous Mater.* **2006**, *93*, 134.
36. Jesudoss, S. K.; Vijaya, J. J.; Kaviyarasu, K.; Kennedy, L. J.; Ramalingam, R. J.; Al-Lohedam, H.; *RSC Adv.* **2018**, *8*, 481.
37. Mohamed, M. M.; Zidan, F. I.; Thabet, M.; *Microporous Mesoporous Mater.* **2008**, *108*, 193.
38. Panpa, W.; Jinawath, S.; *Appl. Catal., B* **2009**, *90*, 389.
39. Naskar, M. K.; Kundu, D.; Chatterjee, M.; *J. Am. Ceram. Soc.* **2012**, *95*, 925.
40. Dey, K. P.; Ghosh, S.; Naskar, M. K.; *Ceram. Int.* **2013**, *39*, 2153.
41. Sánchez-Flores, N. A.; Pacheco-Malagón, G.; Perez-Romo, P.; Armendáriz, H.; Guzmán-Castillo, M. L.; Saniger, J. M.; Fripiat, J. J.; *J. Colloid Interface Sci.* **2008**, *323*, 359.
42. Pérez-Romo, P.; Armendáriz-Herrera, H.; Valente, J. S.; Guzmán-Castillo, M. L.; Hernández-Beltrán, F.; Fripiat, J. J.; *Microporous Mesoporous Mater.* **2010**, *132*, 363.
43. Pacheco-Malagón, G.; Sánchez-Flores, N. A.; Saniger-Blesa, J.; Baños, L.; Pérez-Romo, P.; Valente, J. S.; Guzmán-Castillo, M. L.; Hernández-Beltrán, F.; Fripiat, J. J.; *Microporous Mesoporous Mater.* **2007**, *100*, 70.
44. Pacheco-Malagón, G.; Pérez-Romo, P.; Sánchez-Flores, N. A.; Guzmán-Castillo, M. L.; López-Franco, C.; Saniger, J. M.; Hernández-Beltrán, F.; Fripiat, J. J.; *Inorg. Chem.* **2006**, *45*, 3408.
45. Sánchez-Flores, N. A.; Pacheco-Malagón, G.; Perez-Romo, P.; Armendáriz, H.; Guzmán-Castillo, M. L.; Saniger, J. M.; Fripiat, J. J.; *J. Chem. Technol. Biot.* **2007**, *82*, 614.
46. Pacheco-Malagón, G.; Pérez-Romo, P.; Sánchez-Flores, N. A.; Guzmán-Castillo, M. L.; López, C.; Saniger, J. M.; Hernández-Beltrán, F.; Fripiat, J. J.; *Inorg. Chem.* **2005**, *44*, 8486.
47. *Origin*, version 7.5; Origin Lab Corporation, USA, 2003.
48. Engelhardt, G.; Michel, D.; *High-Resolution Solid State NMR of Silicates and Zeolites*; John Wiley and Sons: New York, 1987.
49. Laredo, G. C.; Vega-Merino, P. M.; Pérez-Romo, P.; Navarrete-Bolaños, J.; Trejo-Zárraga, F.; *Pet. Sci. Technol.* **2017**, *35*, 392.
50. Carney, J. R.; Hagemester, F. C.; Zwier, T. S.; *J. Chem. Phys.* **1998**, *108*, 3379.

Submitted: February 24, 2020

Published online: August 18, 2020

